Thermophysical properties of liquid molybdenum in the near-critical region using quantum molecular dynamics

D. V. Minakov,[1,2,*] M. A. Paramonov,[1,2] and P. R. Levashov[1,3]

[1]*Joint Institute for High Temperatures RAS, Izhorskaya 13 bldg 2, Moscow 125412, Russia*

[2]*Moscow Institute of Physics and Technology, 9 Institutskiy per., Dolgoprudny, Moscow Region 141700, Russia*

[3]*Institute of Problems of Chemical Physics RAS, Academician Semenov avenue 1, Chernogolovka, Moscow Region 142432, Russia*

(Received 21 February 2021; accepted 22 April 2021; published 13 May 2021)

We present a comprehensive first-principles study of the thermophysical properties of liquid molybdenum in the near-critical region. The *ab initio* estimate of the molybdenum critical-point parameters is also provided. The robustness of our calculations is confirmed by the excellent agreement with available experiments on shock compression and the successive isentropic expansion of porous samples of molybdenum and several isobaric expansion experiments. We also analyze important thermodynamic properties such as the isochoric and isobaric heat capacity, the Grüneisen parameter, and the speed of sound of liquid molybdenum along the critical isobar up to the critical point.

DOI: 10.1103/PhysRevB.103.184204

I. INTRODUCTION

Knowledge of the physical chemistry of liquid metals is required for a clear understanding of any liquid-metal processing operation [1]. In addition to the traditional interest in the high-temperature equations of state (EOSs) of liquid metals in the fields of metallurgy, astrophysics, planetary physics, controlled thermonuclear fusion research, and engineering, there are promising new applications emerging related to alternative power engineering, impulse technologies, and the development of new materials, and these new applications require a better understanding of the thermophysical properties of liquid metals in the high-temperature domain [2]. Examples of such new technologies may include the use of hot liquid metal as an efficient heat transfer fluid in concentrated solar power systems [3–5], or nanoparticle production by ultrashort laser ablation of metals in a liquid environment [6–12].

It is not surprising, therefore, that a considerable amount of effort has been concentrated on the experimental and theoretical investigation of expanded liquid metals [13–19]. However, despite their scientific and industrial importance, the properties of metals in a liquid state, with few exceptions, are still not as widely known as those of crystalline metals [20]. It is very challenging to obtain accurate and reliable experimental data on the thermophysical properties of most metallic liquids since some of them are too chemically reactive, too refractory, or too scarce [21]. The critical point at low enough temperature and pressure can be studied with conventional static techniques for only a few metals (Hg, Cs, Rb, K, and Na), and even for these, the accuracy of the measured properties is severely limited by the highly reactive nature of metals at high temperatures and by the intractable problems with the control and measurement of temperature in any high-temperature–high-pressure experiment. The latter becomes particularly important in studies close to the critical point where the analysis of experimental data can easily be hampered by the presence of spurious effects due to temperature gradients [22].

Molybdenum is a refractory metal with a normal density of 10.22 g/cm^3 that plays an important role in metallurgy being employed to harden alloys used by aerospace and nuclear industries. It is also used as a pressure standard for ultrahigh-pressure static experiments [23–25]. The main difficulty for the experimental investigation of molybdenum in a liquid state is of course its high melting temperature (2896 K [26]).

Conventional steady-state or quasi-steady-state experimental techniques are generally limited to below 2500 K. Progress in containerless methods of measurements, notably levitation techniques including acoustic, electromagnetic, aerodynamic, and electrostatic techniques, allowed us to broaden the capability of quasistatic methods of measurements to about 3000 K [27,28]. However, the difficulty of handling levitating liquid samples, arising oscillations, and high-temperature luminescence may result in substantial uncertainties in density measurements [29,30].

Dynamic methods of resistive pulse self-heating associated with 10^4–10^{10} K/s heating rates enable us to study both solid and liquid states of metals and alloys up to 10^4 K, i.e., they allow us to reach the critical point domain. Thus, measurements using this technique are the main source of the thermophysical properties of refractory metals, and molybdenum in particular, in a liquid state. However, the experimental data may be difficult to interpret because of the complexity of the underlying physical phenomena [31–36]. This leads to strong contradictions in the measurement results. For example, the density of molten molybdenum varies from 9.35 to 9.0 g/cm^3 in dynamic experiments. The slope of the thermal expansion curve is also inconsistent [from -0.44 to -0.75 g/(cm^3 K)] [37]. It is not surprising, therefore, that there exists an enormous range of estimates of the critical point—more than twofold

*minakovd@ihed.ras.ru

on temperature (from 8 to 19.7 kK), threefold on density, and several dozen kilobars on pressure.

Another type of dynamic experiment that allows us to investigate the near-critical region is isentropic expansion of shock-compressed substances. The entry of isentropes into the two-phase liquid-vapor domain is accompanied by vaporization, resulting in a change in the slope of the experimental pressure dependences on the unloading wave velocity [37]. This fact is sometimes used to estimate the boundary of the two-phase liquid-vapor domain and the critical parameters [38,39]. The drawback of this method is that typical shock-wave measurements allow us to determine only pressure, internal energy, and density. Only a few temperature measurements in shocked metals are available [40], as well as analogous measurements in release isentropic waves [38].

Thus, the lack of reliable experimental data is the main problem for constructing a reliable semiempirical multiphase EOS of molybdenum in the lower-density and moderate-pressure domain [37]. On the other hand, a theoretical description of molybdenum in a condensed state is very challenging as well. Like many transition metals, it has a complex electronic structure that leads to a variety of unusual physical effects, such as a positive sign of the Seebeck and Hall coefficient near the ambient conditions, anomalous self-diffusion behavior near the melting point [41], dynamical stabilization of the crystal structure at high temperature by anharmonic effects [42], etc. Moreover, the nature of interatomic interaction in molybdenum must change due to the variation in the electron density when going from a liquid to a gaseous state [43]. All of these facts make it virtually impossible to create an adequate analytic model of the thermophysical properties of hot expanded molybdenum without taking into account the influence of electronic structure [44].

Density functional theory (DFT) has now become the preferred method for electronic structure theory for complex chemical systems, especially for metals [45]. First-principles molecular dynamics, also referred to as quantum molecular dynamics (QMD) or *ab initio* molecular dynamics, is widely used nowadays for calculation of the thermophysical properties of condensed matter, both in crystal and unordered states. QMD does not rely upon any empirical data except for fundamental physical constants, so it can be considered as a reference method for analyzing available experimental data and obtaining new data for areas in the phase diagram for which experimental data are unavailable. QMD has already been successfully implemented for the description of thermodynamical and transport properties of hot expanded aluminum [46], boron [47], nickel [48], calculation of the phase diagram of tantalum [49], and estimation of the critical point of tungsten [50]. An extensive *ab initio* study on the thermoelectric transport properties of solid and liquid molybdenum was recently presented by French and Mattsson [51].

In this work, we present a comprehensive first-principles study of the thermophysical properties of liquid molybdenum in the near-critical region. Available experimental data on the isentropic expansion of porous samples are also analyzed and discussed. The critical point of molybdenum is estimated from QMD data. Some important thermodynamic characteristics in the liquid phase, such as the isochoric and isobaric heat capacity, the Grüneisen parameter, and the speed of sound, are also provided.

II. CALCULATION PARAMETERS

All QMD calculations were carried out within the density functional theory (DFT) using a plane-wave basis set, as implemented in the Vienna Ab Initio Simulation Package (VASP) [52–55]. The electron wave functions were expanded by plane waves with an energy cutoff of 400 eV.

The Perdew-Burke-Ernzerhof (PBE) form of the generalized gradient approximation (GGA) was chosen to describe exchange-correlation (XC) effects [56,57]. The electron-ion interaction was treated using the projector augmented wave (PAW) method [58,59] with six valence electrons. The thermal electronic excitations were taken into account by using Fermi-Dirac smearing. A sufficient number of bands was taken so that the occupation of the highest band was less the 10^{-5}, thus up to 1700 orbitals were involved in the near-critical region calculations. The Baldereschi mean-value [60] **k**-point $\{1/4, 1/4, 1/4\}$ was used for the representation of the Brillouin zone. All QMD simulations were done in a canonical (NVT) ensemble using the Nosé-Hoover [61] thermostat. The time step was 2 fs. Each thermodynamic state was typically simulated within no less than 3000 steps. Convergence of the thermodynamic quantities for liquid molybdenum on the number of atoms in the simulation cell was accurately checked in our previous work [62]. We used 128 atoms in all our simulations, except for densities 1.5 and 1.25 g/cm^3, where we dropped the number of atoms to 54 but we refined the Brillouin zone sampling by using a $2 \times 2 \times 2$ Monkhorst-Pack **k**-point mesh.

III. METHODS

A. Interpretation of shock-wave data

For the interpretation of shock-wave experimental data, we use equilibrium methods that were detailed and successfully implemented in our previous works [63,64]. The Rankine-Hugoniot equation is used for the reconstruction of solid and porous Hugoniots. The Rankine-Hugoniot relation connects thermodynamic quantities after and before the shock front (the initial state parameters are denoted by a subscript 0):

$$H(P, \rho, E) = E - E_0 + \frac{1}{2}\left(\frac{1}{\rho} - \frac{m}{\rho_0}\right)(P + P_0) = 0, \quad (1)$$

where E is the specific internal energy, P is the pressure, and ρ is the density. The parameter $m = \rho_0/\rho_{00}$ is the porosity of a sample that connects the initial density of a porous sample ρ_{00} and the reference density of solid molybdenum at the ambient conditions ρ_0. According to the model [65], a heated solid sample is compressed by a shock wave after the instant collapse of the pores at the initial value of pressure.

In shock-compression experiments, two kinematic parameters are determined: the shock-wave velocity in the sample (U_s) and the mass velocity (u_p) behind the shock front. To obtain thermodynamic parameters from U_s and u_p, the laws of

mass and momentum conservation are used:

$$P - P_0 = \frac{\rho_0}{m} U_s u_p, \tag{2}$$

$$\rho = \frac{\rho_0 U_s}{m(U_s - u_p)}. \tag{3}$$

The Hugoniots thus calculated determine the parameters at the initial points of experimental isentropic expansion curves. To restore an entire release isentrope, several approaches with different computational costs are valid [64,66]. In this paper, we use two of them: the method of reshock Hugoniots [64] and Zel'dovich's approach [65]. The latter method is the most useful if many isentropes need to be calculated. To implement the Zel'dovich's approach, the dependence of specific internal energy E on pressure and density is required. Then the following ordinary differential equation for the temperature can be solved with the initial condition $T_H(V_H)$ taken at a Hugoniot curve [67]:

$$\left.\frac{dT}{dV}\right|_S = -T\left(\frac{\partial P}{\partial E}\right)_V. \tag{4}$$

The derivative $(\partial E/\partial P)_V = (\partial E/\partial T)_V/(\partial P/\partial T)_V$ is reconstructed globally based on multiple QMD simulations. The grid of isotherms and isochores is calculated in some region, and then the functions $E(V,T)$ and $P(V,T)$ are interpolated by a bicubic spline. One can use an integration scheme of any order with any step on V for the solution of Eq. (4). The accuracy of the solution can be easily improved by the refinement of the grid of isotherms and isochores. Earlier we applied this approach to reconstruct the release isentropes of tungsten [50], deuterium [68], and aluminum [63].

For comparison with experimental data on isentropic expansion, we use the relation between u_p and pressure P in the form of the Riemann integral [65]:

$$u_p = u_H + \int_{P_H}^{P} \frac{dP}{\rho}\sqrt{\left(\frac{\partial \rho}{\partial P}\right)_S}, \tag{5}$$

where the particle velocity and pressure at the initial state on a Hugoniot curve are denoted as u_H and P_H, respectively.

B. Critical point estimate

The liquid-gas critical point parameters are estimated by the method of successive approach to the critical isotherm; see Fig. 1(a). We calculate a series of supercritical isotherms with gradually decreasing temperatures. Since the critical point is a stationary inflection point on the critical isotherm, we can analyze the density dependence of the derivative $(\partial P/\partial \rho)_T$ on each isotherm and define this point according to two conditions:

$$\left(\frac{\partial P}{\partial \rho}\right)_T = \left(\frac{\partial^2 P}{\partial \rho^2}\right)_T = 0. \tag{6}$$

We need to note here that a small size and short simulation time of a QMD system can lead to a significant statistical error (0.5–1 kbar) of calculated mean pressure [62]. To reduce the influence of this error while determining the critical point, we fit the pressure-temperature data on each isochor by a linear or quadratic function. Supercritical isotherms are then interpolated by a cubic polynomial using the fitted isochoric curves. Thus the parameters of a stationary inflection point can be determined from the solution of a cubic equation.

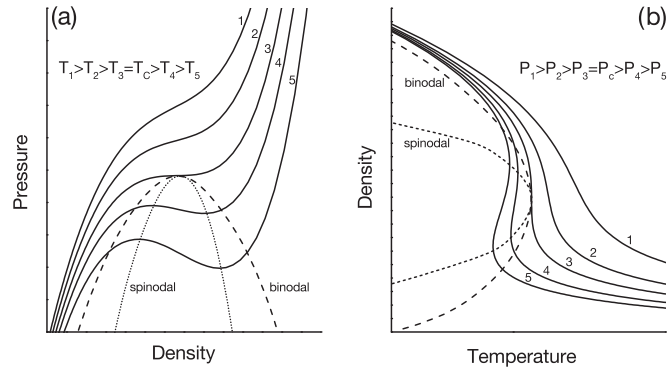

FIG. 1. Schematic phase diagram in the P-ρ and ρ-T planes: (a) method of successive approach to the critical isotherm; (b) method of successive approach to the binodal curve by near-critical isobars.

The averaged critical point parameters and their standard errors in turn are estimated with a Monte Carlo method also referred to as the bootstrap procedure [69]. For each QMD-calculated point at a given temperature and density, we choose random pressure according to the normal distribution with the expectation equal to the calculated pressure and the standard deviation equal to the statistical error. Then we make again the polynomial fitting and inflection point determination as described above. We repeat the whole procedure 3000 times to get statistical significance. The averaging then gives us the estimate of the critical point parameters and their error bars. As the critical isobar is very close to the liquid-gas coexistence curve, Fig. 1(b), we simultaneously obtain the approximate location of the liquid branch of the binodal curve.

IV. RESULTS AND DISCUSSION

A. Interpretation of shock-wave experiments

Molybdenum has been widely studied in shock-wave experiments [70–76]. There are, however, only a few adiabatic release measurements [77,78]. In our simulations, we reproduced solid and some porous Hugoniots, as well as one of the release isentropes corresponding to the unloading of a shock-compressed solid Mo sample and all available data on the adiabatic release response of shock-compressed porous samples with a porosity of $m = 2.31$.

Figure 2 demonstrates the principal and porous shock Hugoniots and release isentropes of molybdenum in the P-ρ diagram. Excellent agreement of the solid QMD Hugoniot with experimental data is observed. However, the situation with porous Hugoniots is more complicated. In Fig. 2 it may be seen that the highest pressure experimental point [70] at 250 GPa for porosity $m = 2.31$ is not reproduced by our calculations. The semiempirical multiphase EOS of molybdenum by Fortov and Lomonosov (FLEOS) [37] predicts a steeper slope of the porous Hugoniot $m = 2.31$ so that the FLEOS curve turns out to be closer to the experimental point at 250 GPa than the QMD one. To clarify this issue,

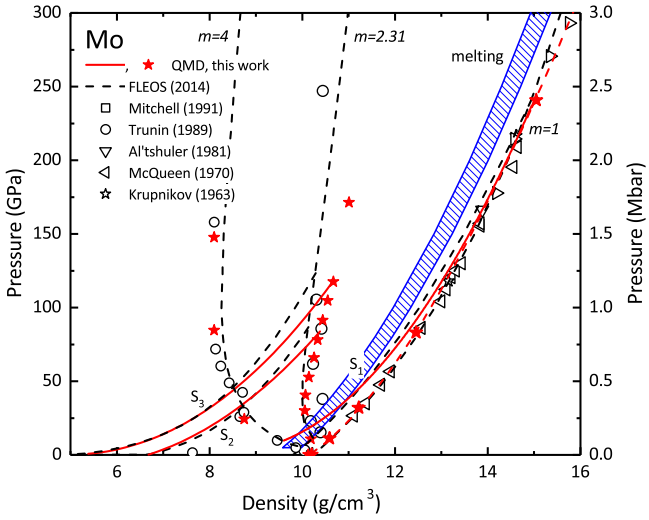

FIG. 2. Shock Hugoniots and release isentropes of solid and porous samples of molybdenum with porosity $m = 2.31$ and 4 in the P-ρ plane. Shock QMD data are shown as red stars, and QMD release isentropes are shown as red lines. Empty symbols are experimental shock-wave measurements [70,73–75,79]. Shock Hugoniots and release isentropes according to FLEOS are shown by the black dashed line for reference. The melting region according to FLEOS is shown by the blue hatched area.

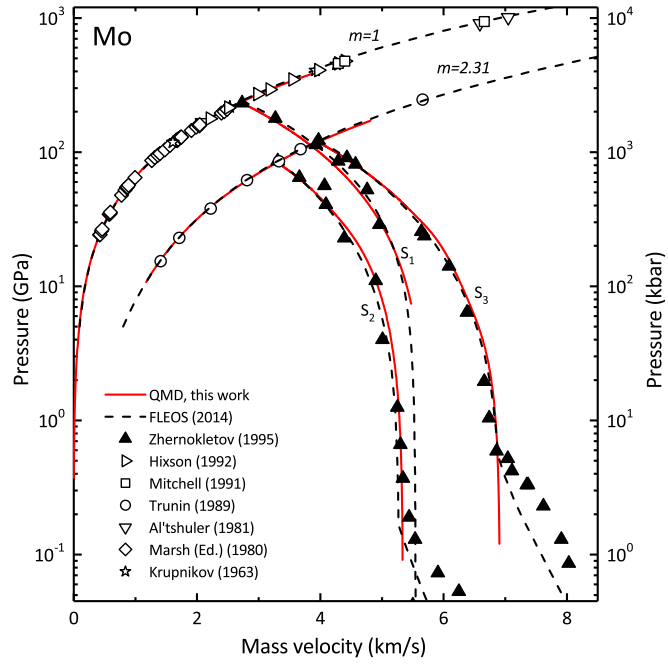

FIG. 3. Shock compression of solid and porous samples of molybdenum and subsequent expansion into different anvil materials in the P-u_p plane; m is the porosity. Experimental points on shock compression [70–75] are shown as empty symbols. Filled triangles are release isentrope measurements by Zhernokletov *et al.* [78]. QMD-calculated Hugoniots and release isentropes are red solid lines with initial points for isentropes corresponding to the experiments [78]. The black dashed lines are according to FLEOS.

we calculated several Hugoniot points for porosity $m = 4$ to check whether it is a systematic overestimation of density of compressed porous samples or just a single point mismatch. As can be seen from Fig. 2, experimental points [70] for this higher porosity are described excellently by our QMD calculations. Thus we can assume that there is no systematic deviation between our calculations and experiments [70] for porous samples.

Three release isentropes were calculated using Eq. (4) with initial conditions at different shock Hugoniots: for S_1 at the point with $u_H = 2.7$ km/s at the principal Hugoniot, and for S_2 and S_3 at the points with $u_H = 3.31$ and 3.97 km/s, respectively, at the Hugoniot with $m = 2.31$. Isentropes S_2 and S_3 are shown in Fig. 2. The first release isentrope S_1 was calculated using the method of reshock Hugoniots [64], while S_2 and S_3 were calculated by the global reconstruction as described in Sec. III. The QMD EOS table, which was used for the global reconstruction, is presented in the supplemental material [80].

The particle velocity for each isentrope was calculated using Eq. (5). The comparison with experimental data is shown in Fig. 3. As can be seen from the figure, our release isentropic curves are in very good agreement with the experimental data by Zhernokletov *et al.* [78] and with FLEOS. However, QMD isentropes S_2 and S_3 do not reproduce the kinks in the experimental dependences. A change in slope of an experimental isentrope may occur due to the partial evaporation (in the case of entry from the liquid phase), so the substance is in a nonhomogeneous state at low pressures. It is believed that the evaporation process is nonequilibrium due to uneven energy distribution in a hot expanded substance [81]. Another explanation considers the formation of jets caused by the reflection of a shock wave at the rough back surface of a porous sample [82]. The FLEOS isentropes (black dashed lines in Fig. 3) take into account the effect of equilibrium evaporation, so that the kinks determine the position of the binodal curve. The thermodynamics of the slope discontinuity at the phase boundary is described in detail in early studies [83,84]. Actually, the experimental kinks were used for the calibration of FLEOS; the FLEOS release isentropes change their slope at pressures of 1.67 and 5.48 kbar for S_2 and S_3, respectively [37]. Our QMD isentropic curves at low pressure correspond to the metastable liquid state due to the small size of the system and the short simulation time, and thus they do not have kinks.

We also present the temperature-density diagram for porous Hugoniot $m = 2.31$ and the corresponding release isentropes S_2 and S_3 in Fig. 4. Despite good agreement in the previous figure, a strong difference between QMD and FLEOS is observed in the T-ρ plane. Since there are no experimental measurements of temperature in isentropic expansion experiments, we can only provide a comparison with the EOS. As can be seen, FLEOS predicts higher temperature in release waves at the same density as QMD; a possible explanation for this is that FLEOS gives lower heat capacity values in the liquid state (see also Sec. IV C). The QMD-predicted critical isobar is also shown in Fig. 4, and it will be discussed in detail below. Thus, it is also noticeable that the QMD entry temperature to the two-phase region for the studied release isentropes will be lower than the FLEOS one.

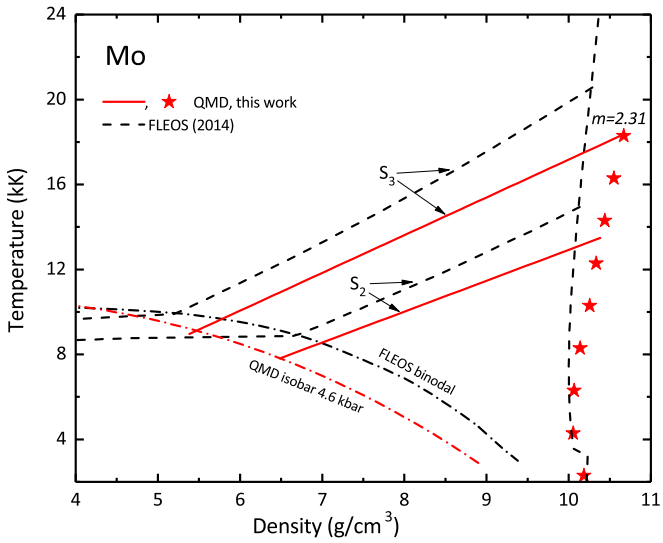

FIG. 4. Shock compression and expansion of porous samples of molybdenum in the T-ρ plane. Shock QMD data are shown as red stars, QMD release isentropes are shown as solid red lines, and the dash-dotted red line is the QMD critical isobar. The dashed and dash-dotted black lines are according to FLEOS.

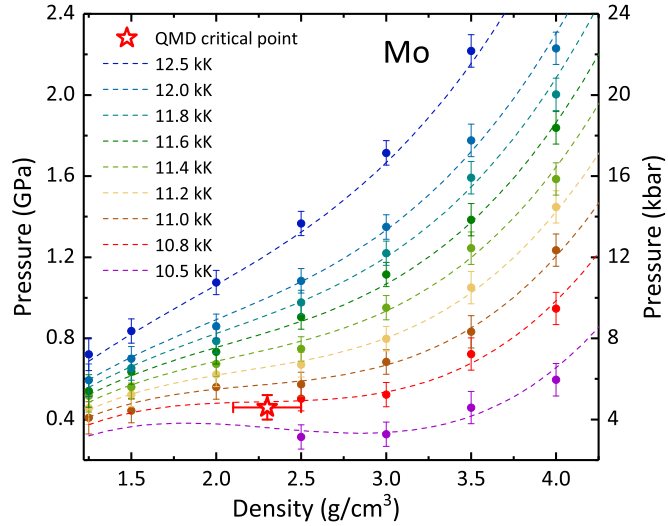

FIG. 6. QMD-calculated pressure with respect to density for molybdenum. Circles are QMD data, while dashed lines are cubic approximations of isotherms calculated from linear approximations of isochores. The estimate of the critical point with error bars is shown as the red star.

B. Investigation of subcritical and supercritical areas

To obtain an accurate *ab initio* EOS of liquid molybdenum in the subcritical and supercritical regions, we calculate a set of isochores in the range of densities from 1.25 to 7 g/cm^3. We have previously presented our *ab initio* EOS data table for Mo for densities higher than 7.35 g/cm^3, and we have shown that QMD can successfully describe some pulse heating and electrostatic levitation experiments; see Ref. [62]. The isochores calculated in this work are shown in Fig. 5. A drastic change in the slopes and intersections of low-density isochores indicates the presence of the critical point region. More accurately, this region can be analyzed from the behavior of supercritical and subcritical isotherms presented in Fig. 6. We calculated a number of points along isotherms at densities from 5 to 1.25 g/cm^3. Temperatures from 12.5 kK and below were taken to reveal oscillations on isotherms in the near-critical region. We strictly ensured that we have a homogeneous state in all our QMD simulations at the near-critical conditions. In fact, we detected a loss of homogeneity and the appearance of a void for temperatures below 10.5 kK, so we had to restrict our analysis to this temperature. Calculations detected a critical isotherm in the vicinity of 11 kK. We performed the polynomial fitting and inflection point determination using the Monte Carlo simulation described in Sec. III B to obtain smooth isothermal curves and to estimate the critical parameters and their errors. Thus we obtained the following parameters of the critical point of molybdenum: $T_c = 10.73 \pm 0.12$ kK, $\rho_c = 2.3 \pm 0.2$ g/cm^3, and $P_c = 4.6 \pm 0.7$ kbar. The critical compressibility factor is $Z_c = P_c\mu/\rho RT_c = 0.22 \pm 0.03$, where μ is the molar mass of molybdenum and R is the universal gas constant. The influence of simulation parameters on the near-critical isotherms and critical point is presented in Appendix.

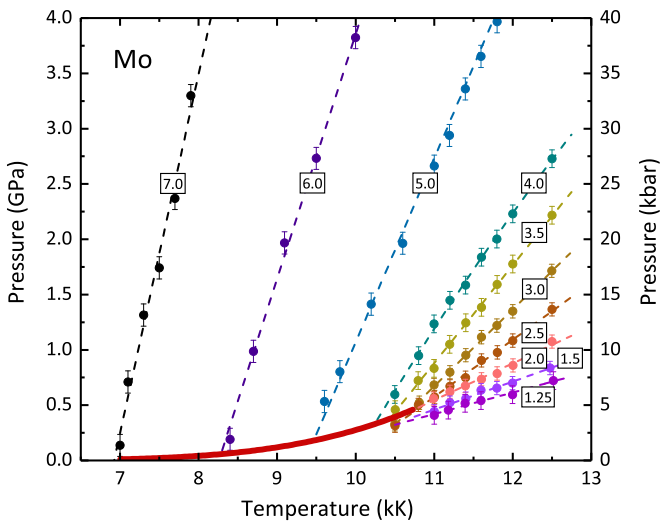

FIG. 5. QMD-calculated pressure with respect to temperature along isochores for liquid molybdenum. Lines are linear and quadratic polynomial fits for isochores [densities (in g/cm^3) are shown in rectangles]. The solid red line is an approximation of the Hultgren [85] data with the QMD-estimated critical point at the end.

An accurate experimental determination of the critical parameters of most metals is impossible due to very extreme conditions [86]. The available critical point estimates for molybdenum vary from 8 to 20 kK for temperature and from 1.0 to 3.7 g/cm^3 for density [15,37,39,87–96]. The lowest and highest values for temperature are given by the estimates of Gathers [15] and Kopyshev [97], respectively, and the equation of state [37] gives the highest critical density. We have collected available estimates of the critical parameters for molybdenum in Table I.

Hereafter, the obtained critical pressure $P_c = 4.6$ kbar is used for the estimation of the liquid-gas coexistence curve.

TABLE I. Estimations of the critical parameters of molybdenum.

Authors	T_c (kK)	ρ_c (g/cm^3)	P_c (kbar)
Kopyshev and Medvedev [97]	19.72		25.15
Hess and Schneidenbach [87]	18.766		29.3
Grosse [98]	17.00		
Fortov *et al.* [88]	16.14	3.18	12.63
Young and Alder [89]	14.59	2.61	11.84
Seydel *et al.* [90]	14.3	3.02	5.68
Khomkin and Shumikhin [91]	12.87	2.8	22.4
Emelyanov *et al.* [39]	12.5 ± 1		10 ± 1
Martynyuk and Tamanga [99]	11.33	1.37	1.75
Seydel and Fucke [92]	11.15 ± 0.55	2.63	5.46 ± 1.16
Martynyuk [93]	10.78	2.47	6.92
This work	10.73 ± 0.12	2.3 ± 0.2	4.6 ± 0.7
Baikov and Shestak [94]	10.4		
Fortov and Lomonosov [37]	10.18	3.69	7.59
Levashov *et al.* [95]	9.6	1.73	4.32
Gathers [15]	8	2.31	9.7
Young [96]	8	1.02	9.7

The critical isobar was accurately reconstructed using linear and quadratic polynomial fits of our QMD isochores. It is presented in Fig. 7. The near-melting region with experimental isobaric expansion data (IEX) [15,100–106] was discussed in our previous work [62]. The best polynomial fit for our critical isobar in the range of temperatures $T_m = 2896 \leqslant T \leqslant 10\,730$ K $= T_c$ is

$$T = A_1(\rho/\rho_0)^3 + B_1(\rho/\rho_0)^2 + C_1(\rho/\rho_0) + D_1, \qquad (7)$$

where $A_1 = -5941.85894$, $B_1 = -10527.01079$, $C_1 = 5701.8218$, $D_1 = 10047.63496$, and $0.879 \geqslant \rho/\rho_0 \geqslant 0.227$. We use $\rho_0 \equiv \rho_0^{\rm QMD} = 10.126$ g/cm^3 in the case of the QMD data, because the calculated density at normal conditions differs slightly from the experimental value.

The FLEOS binodal curve is also shown in Fig. 7. The slope of the binodal and, consequently, FLEOS low-pressure isobars is flatter than that of the QMD critical isobar. Thus, FLEOS does not agree with any available IEX data in the liquid phase. We assume again that this is connected to the underestimation of the heat capacity of liquid in FLEOS [see Sec. IV C and Eq. (12) below].

Some critical point estimates are also shown in Fig. 7. It can be seen that our estimation of the critical point of molybdenum in the ρ/ρ_0-T plane is close to the experimental estimation made by Seydel and Fucke [92] using submicrosecond resistive pulse heating of wire-shaped metallic samples in a highly incompressible medium; the critical temperature was calculated on the basis of an equation for the spinodal derived by Skripov [107]. A very close value of the critical temperature and density was predicted by Martynyuk [93] ($T_c = 10.78$ kK, $\rho_c = 2.47$ g/cm^3, $P_c = 6.92$ kbar) from the analysis of all available experimental data at that time. It is worth noting that all estimates using the soft-sphere model [15,95,96] lie in the left-hand region from our value and underestimate the temperature and density in comparison with the experiment [39,92,98]. It is also interesting to observe significant differences in the estimation of the critical point by the soft-sphere model [96] ($T_c = 8$ kK, $\rho_c = 1.02$ g/cm^3, $P_c = 9.7$ kbar) and the hard-sphere van der Waals model [89] ($T_c = 14.59$ kK, $\rho_c = 2.61$ g/cm^3, $P_c = 11.84$ kbar), both made by the same author. In the experimental study by Emelyanov *et al.* [39], only temperature and pressure were measured in the vicinity of the critical point.

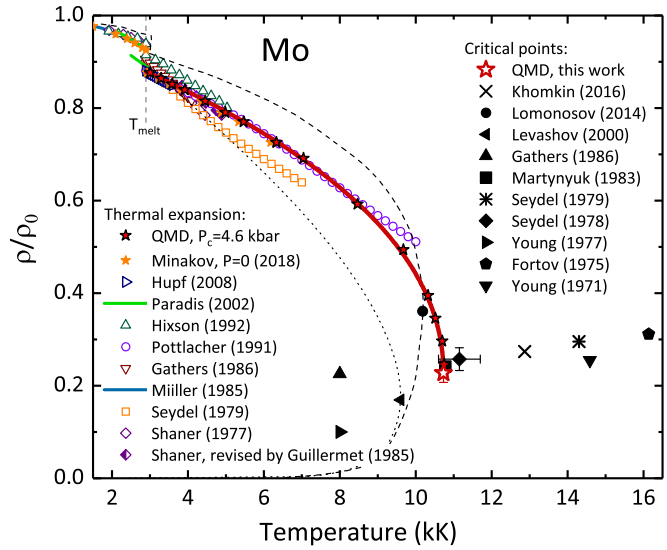

FIG. 7. Phase diagram of molybdenum at low densities in the relative density vs temperature diagram. QMD data: orange stars are the zero-pressure isobar [62]; red line with stars is the 4.6 kbar critical isobar. The IEX experimental data: microsecond and submicrosecond pulse-heating measurements [15,100–104] are shown by empty symbols, millisecond pulse heating [105] is the dark blue line, and electrostatic levitation [106] is the light green line. The FLEOS binodal is the dashed line. Soft sphere prediction of the binodal by Levashov [95] is the dotted line. Critical point estimates: this work is the red star; Khomkin [91] (cross), Fortov and Lomonosov [37] (filled circle), Levashov *et al.* [95] (filled left triangle), Gathers [15] (filled triangle), Martynyuk [93] (filled square), Seydel and Kitzel [90] (asterisk), Seydel and Fucke [92] (filled diamond), Young [96] (right triangle), Fortov *et al.* [88] (filled pentagon), and Young and Alder [89] (filled down-triangle).

Both our critical point and the saturated vapor pressure data of Hultgren [85] can be described well using the empirical relation [108]

$$\ln P = A_2 + B_2/T + C_2 \ln(T), \qquad (8)$$

where the coefficients are $A_2 = 15.901\,42$, $B_2 = -75\,784.721\,56$, $C_2 = -0.043\,68$, P is in bars, and T is in K. The approximation curve is shown in Fig. 5.

C. Heat capacity and Grüneisen parameter

Since we have an accurate *ab initio* EOS table data between the melting and evaporation curves up to the critical temperature, we can examine thermodynamic coefficients or second derivatives of thermodynamic potential. In Fig. 8 we plot isochoric and isobaric heat capacities as a function of temperature along the critical isobar. Isochoric heat capacity was calculated using internal energy along isochores $C_V = (\partial E/\partial T)_V$. To derive a smooth function of isobaric heat capacity $C_P = (\partial H/\partial T)_P$, we approximated the temperature dependence of enthalpy $H = E + PV$ at the critical pressure.

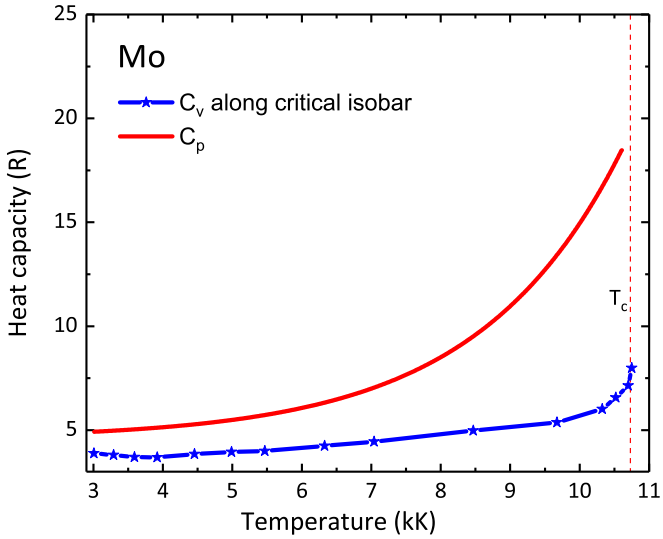

FIG. 8. Isochoric and isobaric heat capacity vs temperature along the critical isobar in liquid Mo.

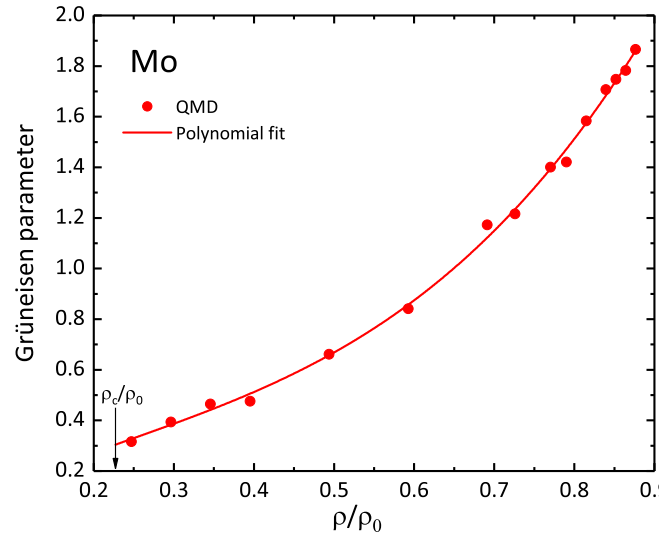

FIG. 9. Grüneisen parameter vs relative density along the critical isobar in liquid Mo.

With the function of linear plus exponential terms, the analytic expression for the enthalpy change in the range of temperatures $T_m = 2896 \leqslant T \leqslant 10\,600$ K is

$$H_T - H_{300} = A_3 + B_3 T + C_3 \exp(D_3 T), \tag{9}$$

where H is given in J/mol, and the coefficients $A_3 = 15\,000$, $B_3 = 38$, $C_3 = 1312.468\,13$, and $D_3 = 4.921\,45 \times 10^{-4}$; $H_{300} = E_{300} + P_c V_0$, the internal energy at 300 K is $E_{300} = -1.048\,912 \times 10^6$ J/mol obtained from QMD [62], and $V_0 = 1/\rho_0$. For C_P we therefore have

$$C_P = B_3 + C_3 D_3 \exp(D_3 T), \tag{10}$$

where C_P is in J/(mol K). As expected, C_P demonstrates a significant growth while approaching the critical point. It is interesting to note a nonmonotonic behavior of isochoric heat capacity. A small segment of decrease after the melting is followed by a noticeable growth at temperatures higher than 4.5 kK, where C_V rises from $2R$ up to $8R$ at the critical temperature. Such high values of heat capacity are determined by strong interparticle interaction and electronic excitations. The last effect includes not only free electrons but also the electrons of inner shells [109]. Therefore, the model of ideal electron gas used in FLEOS for the description of the electronic subsystem underestimates the electronic heat capacity. Another problem of FLEOS is a rough approximation of the number of free electrons as a function of temperature and density; this parameter is ambiguous for a dense medium and depends on the theoretical model in use. Experimental studies of the isochoric heat capacity of liquid metals are generally limited by the low melting temperature of the metals [110–113]. We highlight here the estimation of the $C_V(T)$ dependence for liquid cobalt by Hess *et al.* [114] derived using the experimental isobaric heat capacity, the volume expansion coefficient, and the speed of sound. Experimental dependences are usually limited by the boiling temperature and predict the decrease of C_V with temperature in liquid metals. However, it should be mentioned that current theoretical [115,116] and experimental [117] studies on the isochoric heat capacity in the vicinity of the critical point for inert gases predict significant growth or even divergence at the critical point.

We also calculated the Grüneisen parameter $\gamma = V(\partial P/\partial E)_V$ along the critical isobar. Figure 9 shows γ as a function of relative density ρ/ρ_0 in liquid Mo. We approximated the calculated points with a polynomial fit

$$\gamma = A_4(\rho/\rho_0)^3 + B_4(\rho/\rho_0)^2 + C_4(\rho/\rho_0) + D_4, \tag{11}$$

where $A_4 = 3.169\,25$, $B_4 = -2.259\,31$, $C_4 = 1.661\,91$, and $D_4 = 0.006\,16$.

As can be seen, the Grüneisen parameter exhibits a nonlinear dependence on density and reaches a value of 0.3 at the critical point, which is lower than the ideal gas limit of $\gamma = 2/3$. This result is consistent with previous and recent experimental works on pulsed isochoric heating of gold [118], aluminum [119], and lead [120]. It was shown by Rakhel [119] that this may indicate a strong Coulomb interaction between the particles of a liquid metal resulting in a very high value of the coupling parameter.

Finally, it is possible to calculate one more thermodynamic coefficient: the sound speed. In single-phase states, thermal expansion is related to the Grüneisen coefficient γ, the isobaric heat capacity C_p, and the speed of sound c_s by the expression [121]

$$\left(\frac{\partial \rho}{\partial T}\right)_P = -\frac{\gamma \rho C_p}{c_s^2}. \tag{12}$$

Thus we can check the consistency of the calculated derivatives by a comparison with experimental data on the sound speed at $P = 2$ kbar provided by Hixson and Winkler [101]. Recently, relation (12) was applied by Lomonosov as a criterion of self-consistency between the shock-wave and isobaric expansion experiments [122]. We used the approximation functions (7), (10), and (11) presented above to restore the density dependence of the sound speed of molybdenum along the critical isobar. The corresponding curve is presented in

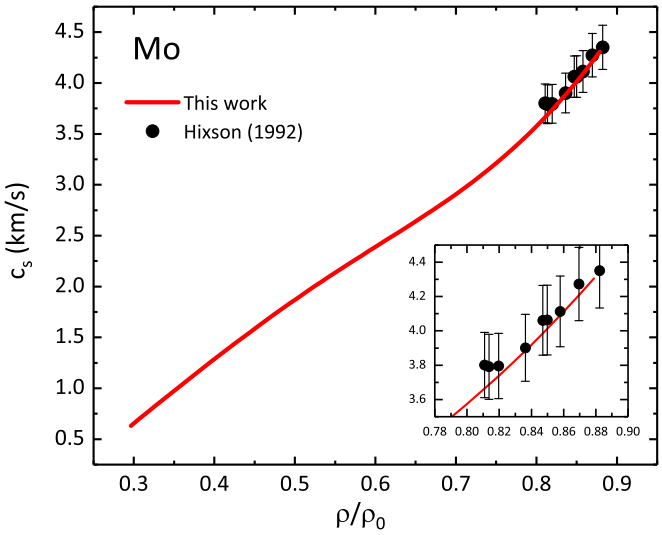

FIG. 10. Speed of sound in liquid molybdenum along the critical isobar. Experimental measurements [101] at 2 kbar are shown as black circles.

Fig. 10. As can be clearly seen from the figure, our curve is in excellent agreement with experimental data.

V. CONCLUSIONS

In this work, we have demonstrated that various experiments for hot expanded molybdenum can be consistently described by a single first-principles method. Our QMD calculations have conclusively reproduced a number of shock Hugoniots and release isentropes for both solid and porous samples. In addition, we have obtained temperature data for shock-wave experiments. In contrast to the semiempirical multiphase EOS by Fortov and Lomonosov [37], we reproduced some IEX experiments in the liquid phase, including the speed of sound measurements by Hixson and Winkler [101]. Also, we discovered that FLEOS gives significantly higher temperatures in an adiabatic expansion in comparison with QMD. We assume that the FLEOS model underestimates the isochoric heat capacity in liquid molybdenum.

We have presented the *ab initio* estimate of the critical parameters of molybdenum: $T_c = 10.73 \pm 0.12$ kK, $\rho_c = 2.3 \pm 0.2$ g/cm^3, and $P_c = 4.6 \pm 0.7$ kbar. Our QMD critical point is close to the experimental estimation of Seydel and Fucke [92] obtained from submicrosecond resistive pulse heating measurements, and to the theoretical prediction of Martynyuk [93], made by a comprehensive analysis of IEX experimental data. We have calculated the critical isobar of molybdenum and estimated the liquid branch of the liquid-gas coexistence curve up to the critical point.

Using our QMD EOS table, we have calculated a number of second derivatives of thermodynamic potential along the critical isobar, including isochoric and isobaric heat capacities, the Grüneisen parameter, and the speed of sound. We have revealed a significant rise in the isochoric heat capacity with temperature; a value as high as $8R$ was obtained in the vicinity of the critical point. On the contrary, the Grüneisen parameter exhibited a substantial drop along the critical isobar, reaching a value of 0.3 well below the ideal-gas limit.

Our entire QMD EOS table for liquid molybdenum is presented in the supplemental material [80].

ACKNOWLEDGMENTS

The authors gratefully thank I. V. Lomonosov for valuable discussions. The authors acknowledge the JIHT RAS Supercomputer Centre, the Joint Supercomputer Centre of the Russian Academy of Sciences, and the Shared Resource Centre "Far Eastern Computing Resource" IACP FEB RAS for providing computing time. This work has been supported by the Russian Science Foundation (Grant No. 20-79-10398).

APPENDIX: CONVERGENCE OF THERMODYNAMIC FUNCTIONS AND INFLUENCE OF COMPUTATIONAL PARAMETERS

1. Dependence on the system size

Preliminary investigation of the near-critical region for Mo was performed using QMD simulations with 54 atoms in the supercell. As can be seen from Fig. 11, further calculations with 128 atoms demonstrate higher pressure along the isotherms, however this difference is decreasing at low densities. We performed several calculations with 250 atoms at $T = 11.2$ kK to check the convergence on the system size, and we noted that increasing the number of atoms to 250 leads to a very slight difference in pressure of about 0.5 kbar. Taking into account an enormous increase of computational costs for first-principles simulations at low densities [123,124], we found it reasonable to use 128 atoms in our main calculations. It should also be noted that the analysis of a stationary inflection point for isotherms obtained with 54 atoms provides an estimate for the critical point as $P_c = 5.6 \pm 0.4$ kbar,

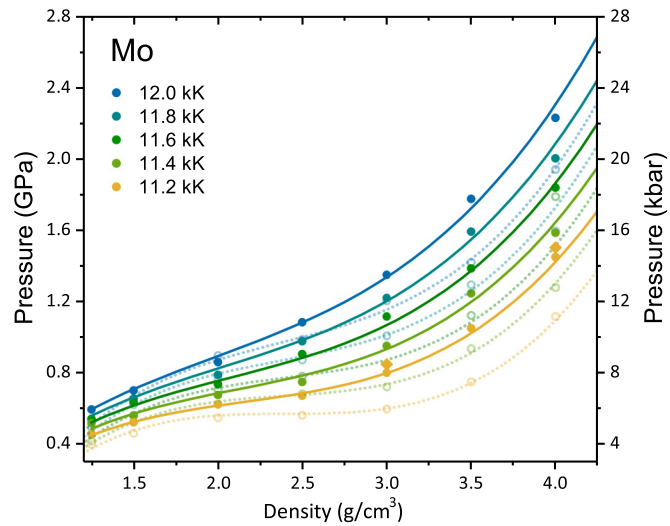

FIG. 11. QMD-calculated supercritical isotherms of Mo. Lines are polynomial approximations. Dotted lines with empty circles are 54 atoms, solid lines with solid circles are 128 atoms, and diamonds are 250 atoms in a supercell. The colors correspond with the temperatures shown in the key.

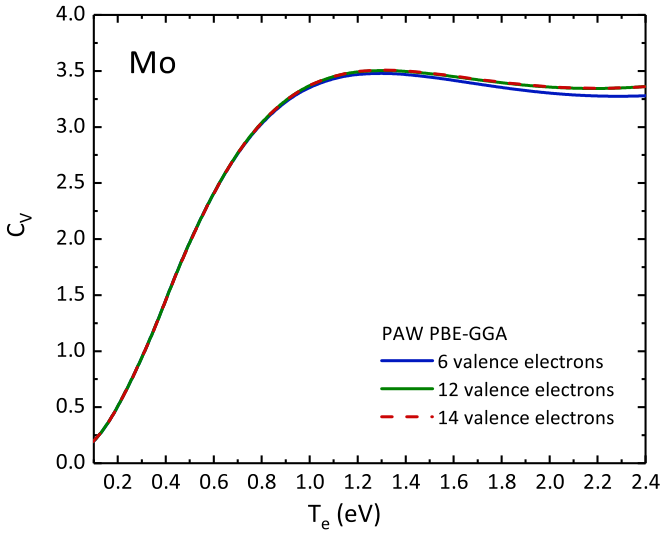

FIG. 12. Isochoric heat capacity of electrons C_V vs temperature of electrons T_e in bcc Mo at normal density. The solid blue line is the PAW potential with six valence electrons, the solid green line is 12 valence electrons, and the dashed red line is 14 valence electrons.

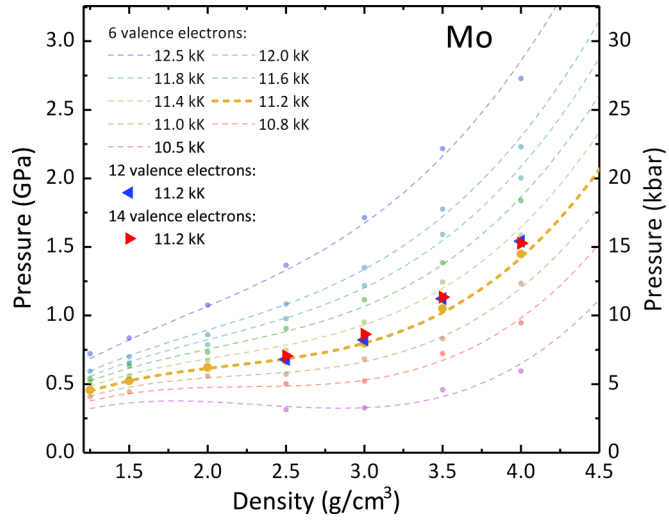

FIG. 13. QMD-calculated supercritical and subcritical isotherms of Mo. Solid circles are six valence electrons, and dashed lines are corresponding polynomial approximations. Blue left triangles are 12 valence electrons, red right triangles are 14 valence electrons.

$T_c = 11.18 \pm 0.07$ kK, and $\rho_c = 2.40 \pm 0.07$ g/cm^3, which is rather close to our final estimate made with 128 atoms.

2. Dependence on the PAW potential

The use of the pseudopotential (PP) approximation with frozen core electrons in DFT calculations may lead to incorrect results at high temperatures due to neglect of thermal excitations of core electrons [109,125,126]. In this regard, we are obliged to analyze the limitations of the pseudopotential in use through a comparison with more accurate pseudopotentials or full-electron calculations. Figure 12 shows the electronic isochoric heat capacity versus electron temperature in bcc molybdenum at normal density calculated using PAW PPs with a different number of valence electrons. As can be seen from the figure, all pseudopotentials demonstrate identical behavior at $T_e < 1.2$ eV; at higher temperatures, the PAW PP with six valence electrons underestimates the heat capacity. The difference between C_V obtained using the six-electron PAW PP and more accurate ones with 12 and 14 valence electrons is about 2% at $T_e = 2$ eV.

Thus, the analysis of heat capacity showed the applicability of PPs at temperatures corresponding to near-critical conditions. Nevertheless, we performed direct QMD calculations of the near-critical isotherm $T = 11.2$ kK with various PPs. Results are presented in Fig. 13. The figure shows that all three PAW PPs provide a consistent description of the near-critical isotherm. We observe only a slight difference of less than 1 kbar at 4 g/cm^3 between the PP with six valence electrons and more accurate ones, and it becomes even more negligible at lower densities.

3. Influence of the exchange-correlation functional

The choice of the exchange-correlation (XC) functional is expected to have the most significant impact on the results of *ab initio* calculations. We use the GGA XC functional with the Perdew-Burke-Ernzerhof (PBE) parametrization [56,57], which does not contain any empirical fitting parameters. The other nonempirical functional that is widely used in QMD calculations nowadays is the Armiento-Mattsson (AM05) functional [127]. The technical difficulty connected with the AM05 functional is the convergence issue of the self-consistent cycle for expanded states [51]. It is very challenging to get long enough QMD trajectories at low densities, so we are forced to limit our analysis to a single isotherm rather than a comparison of critical point estimations. In Fig. 14 we show QMD points calculated using AM05 along the $T = 11.6$ kK isotherm. As can be seen from the figure, AM05 predicts lower pressure than PBE at the same temperature. The difference is about 5.5 kbar at 4 g/cm^3, and

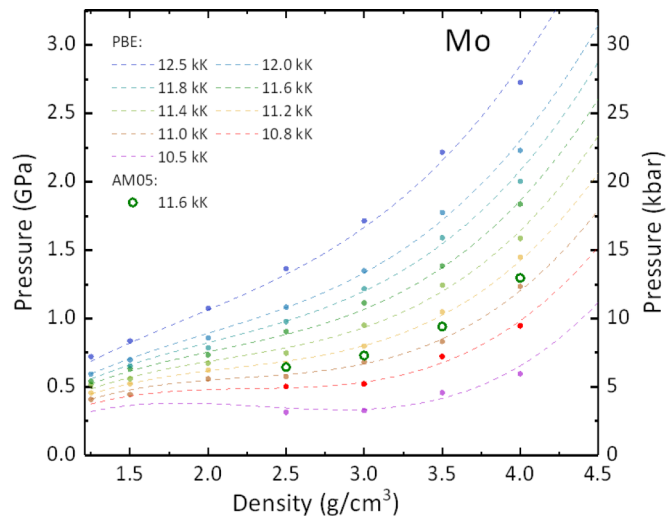

FIG. 14. QMD-calculated supercritical and subcritical isotherms of Mo. Solid circles are the GGA XC-functional with the PBE parametrization, and dashed lines are corresponding polynomial approximations. Open circles are the AM05 XC-functional.

it becomes less at lower densities. On the other hand, the AM05 11.6 kK isotherm is very close to the PBE 11.0 kK isotherm, which, in turn, is very close to the critical one estimated with the use of PBE (10.73 kK). That means that the AM05 11.6 kK isotherm should be very close to the AM05 critical isotherm. So, we can assume with reasonable certainty that the AM05 prediction of the critical temperature may be slightly higher than the PBE one, and AM05 critical pressure and density should be quite close to the PBE estimate. We must stress, however, that these assumptions are very difficult to verify with the current implementation of AM05.

[1] T. Iida and R. Guthrie, *The Physical Properties of Liquid Metals* (Clarendon Press, Oxford, 1988).

[2] T. Daeneke, K. Khoshmanesh, N. Mahmood, I. A. de Castro, D. Esrafilzadeh, S. J. Barrow, M. D. Dickey, and K. Kalantar-zadeh, Chem. Soc. Rev. **47**, 4073 (2018).

[3] N. Lorenzin and A. Abánades, Int. J. Hydrogen Energy **41**, 6990 (2016).

[4] A. Heinzel, W. Hering, J. Konys, L. Marocco, K. Litfin, G. Müller, J. Pacio, C. Schroer, R. Stieglitz, L. Stoppel, A. Weisenburger, and T. Wetzel, Energy Technol. **5**, 1026 (2017).

[5] C. Amy, D. Budenstein, M. Bagepalli, D. England, F. DeAngelis, G. Wilk, C. Jarrett, C. Kelsall, J. Hirschey, H. Wen, A. Chavan, B. Gilleland, C. Yuan, W. C. Chueh, K. H. Sandhage, Y. Kawajiri, and A. Henry, Nature (London) **550**, 199 (2017).

[6] M. E. Povarnitsyn, T. E. Itina, P. R. Levashov, and K. V. Khishchenko, Phys. Chem. Chem. Phys. **15**, 3108 (2013).

[7] S. Ibrahimkutty, P. Wagener, T. d. S. Rolo, D. Karpov, A. Menzel, T. Baumbach, S. Barcikowski, and A. Plech, Sci. Rep. **5**, 16313 (2015).

[8] J. Tomko, J. J. Naddeo, R. Jimenez, Y. Tan, M. Steiner, J. M. Fitz-Gerald, D. M. Bubb, and S. M. O'Malley, Phys. Chem. Chem. Phys. **17**, 16327 (2015).

[9] M. Dell'Aglio, R. Gaudiuso, O. De Pascale, and A. De Giacomo, Appl. Surf. Sci. **348**, 4 (2015).

[10] J. Xiao, P. Liu, C. X. Wang, and G. W. Yang, Prog. Mater. Sci. **87**, 140 (2017).

[11] D. Zhang, B. Gökce, and S. Barcikowski, Chem. Rev. **117**, 3990 (2017).

[12] C.-Y. Shih, R. Streubel, J. Heberle, A. Letzel, M. V. Shugaev, C. Wu, M. Schmidt, B. Gökce, S. Barcikowski, and L. V. Zhigilei, Nanoscale **10**, 6900 (2018).

[13] V. Y. Ternovoi, A. S. Filimonov, S. V. Kvitov, A. A. Pyalling, D. N. Nikolaev, Y. E. Gordon, and V. E. Fortov, High Temp. High Press. **34**, 73 (2002).

[14] H. Hess, A. Kloss, A. Rakhel, and H. Schneidenbach, Int. J. Thermophys. **20**, 1279 (1999).

[15] G. R. Gathers, Rep. Prog. Phys. **49**, 341 (1986).

[16] T. Hüpf, C. Cagran, and G. Pottlacher, EPJ Web Conf. **15**, 01018 (2011).

[17] I. V. Lomonosov and S. V. Fortova, High Temp. **55**, 585 (2017).

[18] E. M. Apfelbaum and V. S. Vorob'ev, J. Phys. Chem. B **119**, 11825 (2015).

[19] E. M. Apfelbaum, Contrib. Plasma Phys. **59**, e201800148 (2019).

[20] Y. Marcus, Special issue on volume properties, J. Chem. Thermodyn. **109**, 11 (2017).

[21] T. Iida and R. I. L. Guthrie, *The Thermophysical Properties of Metallic Liquids: Fundamentals* (Oxford University Press, New York, 2015), Vol. 1.

[22] F. Hensel and H. Uchtmann, Annu. Rev. Phys. Chem. **40**, 61 (1989).

[23] H. K. Mao, P. M. Bell, J. W. Shaner, and D. J. Steinberg, J. Appl. Phys. **49**, 3276 (1978).

[24] J. A. Moriarty, Phys. Rev. B **45**, 2004 (1992).

[25] F. Jona and P. M. Marcus, J. Phys.: Condens. Matter **17**, 1049 (2005).

[26] *CRC Handbook of Chemistry and Physics, Internet Version 2005*, edited by D. R. Lide (CRC, Boca Raton, FL, 2005).

[27] M. Boivineau and G. Pottlacher, Int. J. Mater. Prod. Technol. **26**, 217 (2006).

[28] T. Ishikawa, P.-F. Paradis, T. Itami, and S. Yoda, Meas. Sci. Technol. **16**, 443 (2005).

[29] H. Yoo, C. Park, S. Jeon, S. Lee, and G. W. Lee, Metrologia **52**, 677 (2015).

[30] S. Ozawa, Y. Kudo, K. Kuribayashi, Y. Watanabe, and T. Ishikawa, Mater. Trans. **58**, 1664 (2017).

[31] K. V. Khishchenko, S. I. Tkachenko, P. R. Levashov, I. V. Lomonosov, and V. S. Vorob'ev, Int. J. Thermophys. **23**, 1359 (2002).

[32] K. V. Khishchenko, S. I. Tkachenko, V. E. Fortov, P. R. Levashov, I. V. Lomonosov, and V. S. Vorob'ev, in *DENSE Z-PINCHES: 5th International Conference on Dense Z-Pinches*, edited by C. Deeney, N. R. Pereira, and J. Davis, AIP Conf. Proc. 651 (AIP, Melville, NY, 2002), p. 313.

[33] A. G. Rousskikh, R. B. Baksht, S. A. Chaikovsky, A. V. Fedunin, K. V. Khishchenko, A. Y. Labetsky, P. R. Levashov, A. V. Shishlov, and S. I. Tkachenko, IEEE Trans. Plasma Sci. **34**, 2232 (2006).

[34] S. I. Tkachenko, Tech. Phys. Lett. **28**, 637 (2002).

[35] S. I. Tkachenko, High Temp. **39**, 195 (2001).

[36] A. G. Rousskikh, R. B. Baksht, A. Y. Labetskii, V. I. Oreshkin, A. V. Shishlov, and S. A. Chaikovskii, Plasma Phys. Rep. **30**, 944 (2004).

[37] V. E. Fortov and I. V. Lomonosov, Phys. Usp. **57**, 219 (2014).

[38] A. N. Emelyanov, A. A. Pyalling, and V. Y. Ternovoi, Int. J. Thermophys. **26**, 1985 (2005).

[39] A. N. Emelyanov, D. N. Nikolaev, and V. Ya. Ternovoi, High Temp.–High Press. **37**, 279 (2008).

[40] C. S. Yoo, N. C. Holmes, M. Ross, D. J. Webb, and C. Pike, Phys. Rev. Lett. **70**, 3931 (1993).

[41] T. R. Mattsson, N. Sandberg, R. Armiento, and A. E. Mattsson, Phys. Rev. B **80**, 224104 (2009).

[42] C. Asker, A. B. Belonoshko, A. S. Mikhaylushkin, and I. A. Abrikosov, Phys. Rev. B **77**, 220102(R) (2008).

[43] M. Aniya, Phys. B **239**, 144 (1997).

[44] E. M. Apfelbaum, Phys. Plasmas **24**, 052702 (2017).

[45] C. J. Cramer and D. G. Truhlar, Phys. Chem. Chem. Phys. **11**, 10757 (2009).

[46] J. Clérouin, P. Noiret, V. N. Korobenko, and A. D. Rakhel, Phys. Rev. B **78**, 224203 (2008).

[47] J. Clérouin, P. Renaudin, and P. Noiret, Phys. Rev. E **77**, 026409 (2008).

[48] J. Clérouin, C. Starrett, G. Faussurier, C. Blancard, P. Noiret, and P. Renaudin, Phys. Rev. E **82**, 046402 (2010).

[49] L. Miljacic, S. Demers, Q.-J. Hong, and A. van de Walle, Calphad **51**, 133 (2015).

[50] D. V. Minakov, M. A. Paramonov, and P. R. Levashov, Phys. Rev. B **97**, 024205 (2018).

[51] M. French and T. R. Mattsson, Phys. Rev. B **90**, 165113 (2014).

[52] G. Kresse and J. Hafner, Phys. Rev. B **47**, 558 (1993).

[53] G. Kresse and J. Hafner, Phys. Rev. B **49**, 14251 (1994).

[54] G. Kresse and J. Furthmüller, Phys. Rev. B **54**, 11169 (1996).

[55] G. Kresse and J. Furthmüller, Comput. Mater. Sci. **6**, 15 (1996).

[56] J. P. Perdew, K. Burke, and M. Ernzerhof, Phys. Rev. Lett. **77**, 3865 (1996).

[57] J. P. Perdew, K. Burke, and M. Ernzerhof, Phys. Rev. Lett. **78**, 1396(E) (1997).

[58] P. E. Blöchl, Phys. Rev. B **50**, 17953 (1994).

[59] G. Kresse and D. Joubert, Phys. Rev. B **59**, 1758 (1999).

[60] A. Baldereschi, Phys. Rev. B **7**, 5212 (1973).

[61] S. Nosé, J. Chem. Phys. **81**, 511 (1984).

[62] D. V. Minakov, M. A. Paramonov, and P. R. Levashov, AIP Adv. **8**, 125012 (2018).

[63] D. V. Minakov, P. R. Levashov, K. V. Khishchenko, and V. E. Fortov, J. Appl. Phys. **115**, 223512 (2014).

[64] M. A. Paramonov, D. V. Minakov, and P. R. Levashov, J. Phys.: Conf. Ser. **946**, 012089 (2018).

[65] Y. B. Zel'dovich and Y. P. Raizer, *Physics of Shock Waves and High-temperature Hydrodynamic Phenomena* (Dover Publications, New York, 2002).

[66] J.-B. Maillet, E. Bourasseau, L. Soulard, J. Clerouin, and G. Stoltz, Phys. Rev. E **80**, 021135 (2009).

[67] Y. B. Zel'dovich, Zh. Eksp. Teor. Fiz **32**, 1577 (1957).

[68] A. V. Chentsov and P. R. Levashov, Contrib. Plasma Phys. **52**, 33 (2012).

[69] B. Efron, Biometrika **68**, 589 (1981).

[70] R. F. Trunin, G. V. Sirnakov, Yu. N. Sutulov, A. B. Medvedev, B. D. Rogozkin, and Yu. E. Fedorov, Zh. Eksp. Teor. Fiz. **96**, 1024 (1989).

[71] R. Hixson and J. Fritz, J. Appl. Phys. **71**, 1721 (1992).

[72] S. P. Marsh, *LASL Shock Hugoniot Data* (University of California Press, Berkeley, CA, 1980).

[73] L. V. Al'tshuler, A. A. Bakanova, I. P. Dudoladov, E. A. Dynin, R. F. Trunin, and B. S. Chekin, J. Appl. Mech. Tech. Phys. **22**, 145 (1981).

[74] A. Mitchell, W. Nellis, J. Moriarty, R. Heinle, N. Holmes, R. Tipton, and G. Repp, J. Appl. Phys. **69**, 2981 (1991).

[75] K. Krupnikov, A. Bakanova, M. Brazhnik, and R. Trunin, Sov. Phys. Dokl. **8**, 205 (1963).

[76] C. E. Ragan, Phys. Rev. A **29**, 1391 (1984).

[77] M. Zhernokletov, G. V. Simakov, Y. N. Sutulov, and R. F. Trunin, Teplofiz. Vys. Temp. **33**, 40 (1995).

[78] M. Zhernokletov, A. Medvedev, and G. Simakov, Khim. Fiz. **14**, 49 (1995).

[79] R. McQueen, S. Marsh, J. Taylor, J. Fritz, and W. Carter, High Veloc. Impact Phenom. **293**, 294 (1970).

[80] See Supplemental Material at http://link.aps.org/supplemental/10.1103/PhysRevB.103.184204 for the QMD EOS tables prepared for the reconstruction of release isentropes and for the reconstruction of the critical isobar in the liquid state.

[81] L. V. Al'tshuler, A. V. Bushman, M. V. Zhernokletov, V. N. Zubarev, A. A. Leont'ev, and V. E. Fortov, Sov. Phys. JETP **51**, 373 (1980).

[82] O. Durand and L. Soulard, J. Appl. Phys. **114**, 194902 (2013).

[83] M. Naval Ordnance Laboratory (White Oak) and U.S.O. of Naval Research, *Proceedings [of the] fourth symposium (international) on detonation: Sponsored by the U.S. naval ordnance laboratory in cooperation with the office of naval research, October 12-15, 1965* (Office of Naval Research, Department of the Navy, 1967), p. 245.

[84] L. V. Al'Tshuler, A. A. Bakanova, A. V. Bushman, I. P. Dudoladov, and V. N. Zubarev, Sov. Phys. JETP **46**, 980 (1977).

[85] R. R. Hultgren, R. L. Orr, P. D. Anderson, and K. K. Kelley, *Selected Values of Thermodynamic Properties of Metals and Alloys* (Wiley, New York, 1963).

[86] G. Pottlacher and H. Jäger, J. Non-Cryst. Solids **205–207**, 265 (1996), Ninth International Conference on Liquid and Amorphous Metals.

[87] H. Hess and H. Schneidenbach, Z. Metallkd. **87**, 979 (1996).

[88] V. E. Fortov, A. N. Dremin, and A. A. Leont'ev, High Temp. **13**, 1072 (1975).

[89] D. A. Young and B. J. Alder, Phys. Rev. A **3**, 364 (1971).

[90] U. Seydel, H. Bauhof, W. Fucke, and H. Wadle, High Temp. High Press. **11**, 635 (1979).

[91] A. L. Khomkin and A. S. Shumikhin, High Temp.–High Press. **46**, 367 (2017).

[92] U. Seydel and W. Fucke, J. Phys. F **8**, L157 (1978).

[93] M. Martynyuk, Zh. Fiz. Khim. **57**, 810 (1983).

[94] A. Baikov and A. Shestak, High Temp. High Press. **18**, 459 (1986).

[95] P. R. Levashov, V. E. Fortov, K. V. Khishchenko, and I. V. Lomonosov, in *Shock Compression of Condensed Matter-1999*, edited by M. D. Furnish, L. C. Chhabildas, and R. S. Hixson, AIP Conf. Proc. 505 (AIP, Melville, NY, 2000), p. 89.

[96] D. A. Young, Soft-sphere model for liquid metals, Tech. Rep. No. UCRL-52352 (University of California, Livermore, CA, 1977).

[97] V. P. Kopyshev and A. B. Medvedev, Sov. Tech. Rev. B **5**, 37 (1993).

[98] A. Grosse, J. Inorg. Nucl. Chem. **22**, 23 (1961).

[99] M. M. Martynyuk and P. A. Tamanga, High Temp. High Press. **31**, 561 (1999).

[100] T. Hüpf, C. Cagran, G. Lohöfer, and G. Pottlacher, J. Phys.: Conf. Ser. **98**, 062002 (2008).

[101] R. S. Hixson and M. A. Winkler, Int. J. Thermophys. **13**, 477 (1992).

[102] G. Pottlacher, E. Kaschnitz, and H. Jager, J. Phys.: Condens. Matter **3**, 5783 (1991).

[103] U. Seydel and W. Kitzel, J. Phys. F **9**, L153 (1979).

[104] J. W. Shaner, G. R. Gathers, and C. Minichino, High Temp. High Press. **9**, 331 (1977).

[105] A. P. Miller and A. Cezairliyan, Int. J. Thermophys. **6**, 695 (1985).

[106] P.-F. Paradis, T. Ishikawa, and S. Yoda, Int. J. Thermophys. **23**, 555 (2002).

[107] V. P. Skripov, *Metastable Liquids* (Wiley, New York, 1974).
[108] H. Hess, Phys. Chem. Liq. **30**, 251 (1995).
[109] P. R. Levashov, G. V. Sin'ko, N. A. Smirnov, D. V. Minakov, O. P. Shemyakin, and K. V. Khishchenko, J. Phys.: Condens. Matter **22**, 505501 (2010).
[110] T. B. Douglas, A. F. Ball, and D. C. Ginnings, J. Res. Nat. Bur. Stand. **46**, 334 (1951).
[111] M. P. Vukalovich, A. I. Ivanov, L. R. Fokin, and A. T. Yakovlev, *Thermophysical Properties of Mercury* (State Committee for Standards at the Board of Minister of the Soviet Union, Moscow, 1971).
[112] C. R. Brooks, Phys. Chem. Liq. **4**, 125 (1974).
[113] I. Makarenko, A. Nikolaenko, V. Ivanov, and S. Stishov, Zh. Eksp. Teor. Fiz. **69**, 1723 (1975).
[114] H. Hess, E. Kaschnitz, and G. Pottlacher, High Press. Res. **12**, 29 (1994).
[115] R. J. Sadus, Phys. Rev. E **99**, 012139 (2019).
[116] S. Pieprzyk, A. C. Brańka, S. Maćkowiak, and D. M. Heyes, J. Chem. Phys. **148**, 114505 (2018).
[117] A. Haupt and J. Straub, Phys. Rev. E **59**, 1795 (1999).
[118] L. V. Al'tshuler, S. E. Brusnikin, and A. I. Marchenko, High Temp. **27**, 492 (1989).
[119] A. D. Rakhel, J. Phys.: Condens. Matter **30**, 295602 (2018).
[120] A. M. Kondratyev, V. N. Korobenko, and A. D. Rakhel, J. Exp. Theor. Phys. **127**, 1074 (2018).
[121] A. B. Medvedev and R. F. Trunin, Phys. Usp. **55**, 773 (2012).
[122] I. V. Lomonosov, in *Shock Compression of Condensed Matter - 2015: Proceedings of the Conference of the American Physical Society Topical Group on Shock Compression of Condensed Matter*, edited by I. Oleynik, S. M Peiris, R. Ravelo, R. Chau, T. Germann, and T. D. Sewel, AIP Conf. Proc. 1793 (AIP, Melville, NY, 2017), p. 050022.
[123] V. Stegailov and V. Vecher, in *International Conference on Parallel Processing and Applied Mathematics* (Springer, Cham, 2017), pp. 81–90.
[124] V. Stegailov, G. Smirnov, and V. Vecher, Concurr. Computat.: Practice Exper. **31**, e5136 (2019).
[125] G. V. Sin'ko, N. A. Smirnov, A. A. Ovechkin, P. R. Levashov, and K. V. Khishchenko, High Energy Density Phys. **9**, 309 (2013).
[126] D. Minakov and P. Levashov, Comput. Mater. Sci. **114**, 128 (2016).
[127] R. Armiento and A. E. Mattsson, Phys. Rev. B **72**, 085108 (2005).